Materials Science and Engineering C 30 (2010) 20–26

Contents lists available at ScienceDirect

Materials Science and Engineering C

journal homepage: www.elsevier.com/locate/msec

Characterization of gold nanoparticle binding to microtubule filaments

Jing C. Zhou [a,1], Xianghuai Wang [b,2], Mei Xue [c], Zheng Xu [a], Toshikazu Hamasaki [d], Yang Yang [a,e], Kang Wang [c,e], Bruce Dunn [a,e,*]

[a] Department of Materials Science and Engineering, University of California, Los Angeles, Engineering V. Los Angeles, CA 90095, USA
[b] Department of Chemistry and Biochemistry, University of California, Los Angeles, Los Angeles, CA 90095, USA
[c] Department of Electrical Engineering, University of California, Los Angeles, Engineering IV. Los Angeles, CA 90095, USA
[d] Department of Bioengineering, University of California, Los Angeles, Engineering V. Los Angeles, CA 90095, USA
[e] The California NanoSystems Institute, University of California, Los Angeles, Los Angeles, CA 90095, USA

ARTICLE INFO

Article history:
Received 17 July 2009
Accepted 13 August 2009
Available online 20 August 2009

Keywords:
Microtubule
Gold nanowires
Biotemplating
Surface enhanced Raman spectroscopy
X-ray photoelectron spectroscopy

ABSTRACT

Microtubule (MT) protein filaments were used as templates for fabricating Au nanowires as a bottom-up approach for fabricating building blocks for future integrated circuits. Photochemical reduction methods were employed to form Au nanoparticles which bind and uniformly cover the MT filaments. Synthesis of the MT-templated Au nanowires was characterized using UV/vis spectroscopy and transmission electron microscopy (TEM). In addition, binding between the MT filaments and Au nanoparticles was investigated using surface enhanced Raman spectroscopy (SERS) and X-ray photoelectron spectroscopy (XPS) to establish the nature of the binding sites. A variety of functional groups were identified by SERS to interact with the Au including imidazole, sulfur, aromatic rings, amine, and carboxylate. The imidazole ring in the histidine is the most prominent functional group for Au binding. The results from these studies provide better understanding of the binding between Au and the biotemplate and give insight concerning methods to improve Au coverage for MT-templated Au nanowires.

1. Introduction

Biological structures are attractive as templates to form nanoscale architectures for electronics because of their size, geometry and ability to interact with inorganic materials. As an alternative to top-down lithography approaches, which are reaching theoretical and practical limits [1,2], biotemplating provides a means of assembling nanoparticles into the conductive nanowires and nanowire arrays that serve as the building blocks for logic and memory devices as well as interconnects and interconnect arrays [1,3–5]. For these reasons, a number of biological filaments including histidine-rich peptides [6], peptide nanotubes [7], DNA [3,8,9], M13 bacterial phage [10–13], tobacco mosaic virus (TMV) [14,15], flagella [16] and amyloid fiber from yeast [17] have been explored as templates for nanowires. The electrical properties of these structures are just beginning to be reported [8,13,17].

Microtubule (MT) filaments have also been investigated as templates for conducting nanowires. These long, filamentous proteins found in eukaryotic cells are rigid hollow cylindrical tubes, 25 nm in diameter and up to 20 μm in length. The filaments are assembled from heterodimer proteins called αβ-tubulin [18]. After assembly, the part of the tubulin surface exposed to the outer surface of the MT contains a number of functional groups that can serve as potential metal binding sites.

A variety of metal nanoparticles have been shown to bind to the MTs including Ag [19], Au [20–22], Pd [20,23], Ni [24,25], and Co [24,25]. The deposition of gold nanoparticles on MTs is of particular interest because of the prospect of forming nanowires as interconnects for device applications. Recently, we reported a method for fabricating MT-templated nanowires with continuous gold coverage, a feature which had not been obtained previously with MT templates. The metallization process is based on the photochemical reduction of Au^{3+} to enlarge the Au nanoparticles previously bound to the MTs [26]. The photochemical reaction utilizes a non-ionic surfactant, Triton X-100 (TX-100), to serve as both a reducing agent and a stabilizing agent that enables Au nanoparticles to be formed in a controlled manner [27,28]. The conductivity values measured for this material are less than bulk gold. One hypothesis for this lower value is that residual TX-100 on the surface of the MT leads to poor inter-particle contact.

Understanding the nature of the interaction between the biological species and the metal surface is essential for the fabrication, properties and stability of the biotemplated structures. For the most part, however, the nature of the binding between metals and biological templates has not been well characterized. In the MT-templated systems, spectroscopic

* Corresponding author. The California NanoSystems Institute, University of California, Los Angeles, Los Angeles, CA 90095, USA.
E-mail address: bdunn@ucla.edu (B. Dunn).
[1] Present address: Center for Bio/Molecular Science and Engineering, Naval Research Laboratory, 4555 Overlook Ave SW, Washington, DC 20375, USA.
[2] Present address: Department of Chemistry and Center for Photochemical Sciences, Bowling Green State University. Bowling Green, Ohio 43403, USA.

0928-4931/$ – see front matter © 2009 Elsevier B.V. All rights reserved.
doi:10.1016/j.msec.2009.08.003

studies concerning protein–metal interactions have yet to appear. Behrens et al. discussed possible Pd binding sites on MT based on the hard and soft acids and bases (HSAB) principle [29] and surface accessibility. Because the four histidine residues that contain nitrogen atoms are the only soft ligands centrally located on αβ-tubulin, these histidines are thought to be potentially responsible for the nucleation of Pd particles from Pd^{2+} ions and for the binding of the Pd nanoparticles [20,23]. This hypothesis was supported by a computer simulation study on nucleation of Pt on proteins and DNA [20,30].

In the current study, we used UV/vis spectroscopy and transmission electron microscopy (TEM) to characterize the Au nanoparticles formed in the presence of MTs. In addition, surface enhanced Raman spectroscopy (SERS) was used to identify the Au binding sites on MTs. We found that aside from the imidazole group in the histidine, other functional groups such as carboxylate, primary amine, sulfur and aromatic rings also contribute to the attachment of Au to MTs. Some of the details of the binding were confirmed using X-ray photoelectron spectroscopy (XPS). The results not only provide insight concerning the nature of biotemplate metallization, they also suggest directions for improving metal coverage on biotemplates.

2. Experimental

2.1. Isolation and polymerization of tubulins

The MTs were assembled from twice cycled αβ-tubulins isolated from porcine brain tissue using procedures modified from the protocol of Williams et al. [31]. The concentration of the tubulins was 2.7 mg/ml. The tubulins were stored at −80 °C in buffer containing 1,4-piperazinediethanesulfonic acid (PIPES) (100 mM; pH 6.8), ethylene glycol-bis (2-aminoethylether)-N,N,N′,N′-tetraacetic acid (EGTA) (1 mM), $MgSO_4$ (2 mM), and dithiothreitol (DTT) (2 mM). To assemble the MTs in vitro, the tubulin aliquots were thawed and mixed with guanosine triphosphate (GTP) (1 mM) and incubated at 37 °C for 30 min. Taxol (20 μM) was added at the end of the incubation to stabilize the MTs and 0.02% NaN_3 was added to prevent bacterial growth.

2.2. Au nanoparticle formation and deposition on MTs

Au nanoparticle formation was based on the photochemical route reported by Pal [28] and modified by us [26]. MT stock solution was

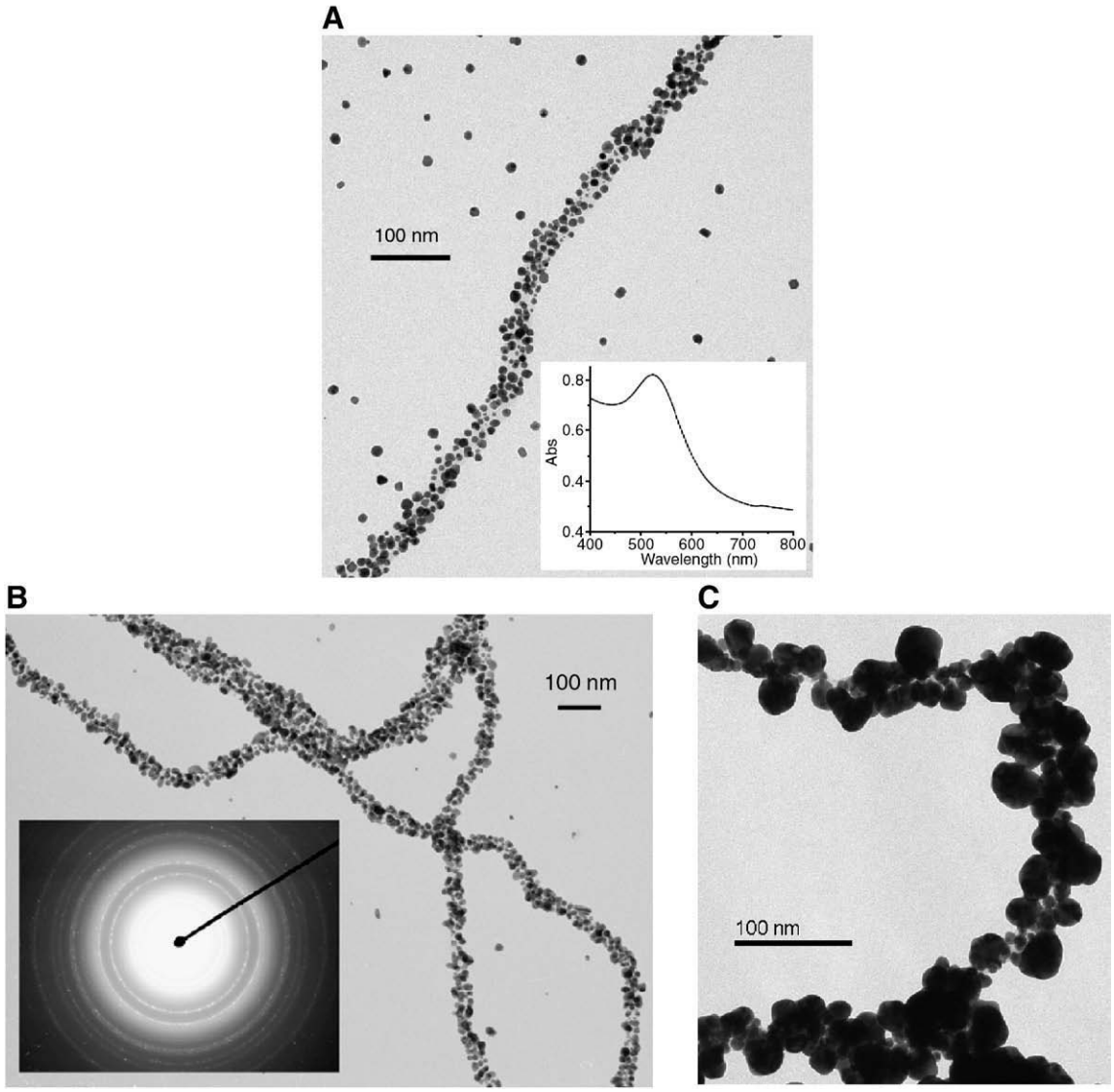

Fig. 1. TEM image of Au decorated MT formed by photochemical reduction methods. (A) Au decorated MT after first UV irradiation. The inset shows a typical UV/vis spectrum of a solution containing MT, $HAuCl_4$ and TX-100 after 5 min exposure to UV. (B) Increased Au coverage on MT after the second UV irradiation. The inset shows the electron diffraction pattern of the region. (C) Au growth on MT after a third UV irradiation using higher concentration of $HAuCl_4$ and no TX-100. These larger Au nanoparticles attached to MTs were used for the SERS measurements.

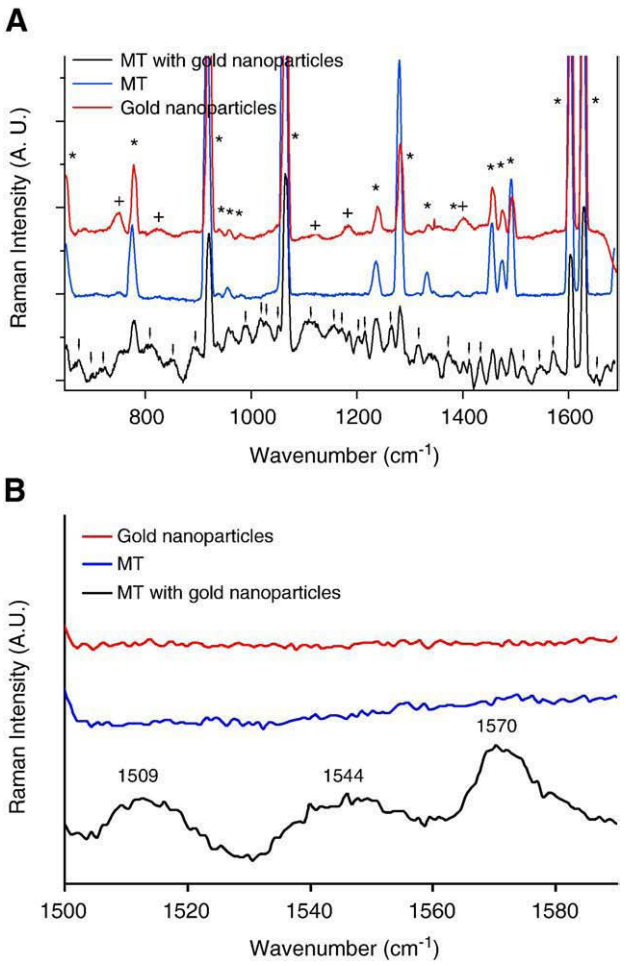

Fig. 2. Raman spectra for the gold–MT system. (A) Raman spectra of MT with gold nanoparticles (black), gold nanoparticles with PIPES buffer and TX-100 (red) and ordinary Raman spectrum of MT in PIPES buffer and TX-100 (blue). The peaks labeled with * are the laser plasma lines. The peaks labeled with + are from the TX-100. The peaks labeled with an arrow are surface enhanced modes of MT protein. (B) Spectra in the region from 1500 cm^{-1} to 1590 cm^{-1} showing enhanced vibrational modes. The peak at 1509 cm^{-1} and 1544 cm^{-1} are assigned to NH_3^+ symmetric deformation mode, and the peak at 1570 cm^{-1} is the C=C stretch of the imidazolium ring [39]. (For interpretation of the references to color in this figure legend, the reader is referred to the web version of this article.)

diluted to 13.5 μg/ml using 20 mM PIPES buffer and 20 μM taxol. 2 mM $HAuCl_4$ and 5 mM TX-100 were added and well mixed into the solution. The mixture was transferred to UV cuvets (Eppendorf) and exposed to 254 nm UV (Fisher Biotech UV Crosslinker FB-UVXL-1000) for 5 min. The solution turned salmon red indicating the formation of Au nanoparticles. The solution was incubated at room temperature overnight to allow Au nanoparticle binding to the MTs. To obtain TEM images (JEOL JEM-1200EX Electron Microscope at 80 kV), 10 μl of the sample solution was adsorbed directly onto formvar coated TEM grids. Electron diffraction pattern was obtained using JEOL JEM-100 CX at 100 kV.

2.3. Sample preparation for surface enhanced Raman spectroscopy

9 ml of the solution containing Au decorated MT prepared as described above was centrifuged at 4000 rpm for 5 min to pelletize the Au MT. The supernatant was discarded and the pellet was resuspended in distilled water. The suspension was centrifuged again and the pellet was resuspended in 800 μl of 20 mM PIPES. 300 μl of 10 mM $HAuCl_4$ was added to the suspension, which was then exposed to the UV irradiation again for 5 min. The resulting Au MT was pelletized and resuspended again in 420 μl of 20 mM PIPES. 180 μl of 10 mM $HAuCl_4$ solution was then added and a third irradiation was performed. The final Au MT sample was pelletized and washed two times in distilled water. It was then concentrated and resuspended in 20 μl distilled water and deposited as a small spot in the center of a 1 cm × 1 cm Si wafer.

Two separate control samples were prepared for the SERS experiments. One control sample consisted of only the Au nanoparticles. This sample was prepared using three photochemical reduction steps, similar to the procedure described above. The centrifugation

Table 1
Assignments for the surface enhanced Raman frequencies for the binding of MTs to the Au nanoparticles.

Frequency (cm^{-1})	Peak assignments	Ref	Frequency (cm^{-1})	Peak assignments	Ref
675	ν(C–S)	[39]	1157	$\omega(NH_3^+)$	[39]
699	ν(S–CH_3) in Met	[42]	1171	Ring in-plane C–H bending	[42,45,46]
718	ν(S–CH_3) in Met	[42]	1202	Ring C–C_β stretching	[36,39,42,43]
812	$\tau(NH_3^+)$	[39]	1215	$\omega(CH_2)$	[37]
853	ν(C–C), $\tau(CH_2)$ or $\rho(NH_3^+)$	[39]	1265	δ(C–C–H)	[39,46]
	$\delta(COO^-)$	[45]			
	Symmetric ring stretching	[42]	1318	$\omega(CH_2)$	[40]
891	ν(C–C)	[37]	1372	ν_s(COOH)	[37,39,45]
993	ν(C–C)	[39]	1413	protonated His ν_s(N–C–N)	[42,44]
	$Phe_{\nu 12}$ ring deformation	[37,39]	1435	$\delta(CH_2)$	[36,40]
1016	ν(C–C)	[39]			
	Benzene/ pyrrole breathing	[42]	1509	$\delta_s(NH_3^+)$	[39]
1033	ν(C–NH_3)	[39]	1544	$\delta_s(NH_3^+)$	[39]
1052	$\tau(NH_3^+)$ or $\omega(CH_2)$	[39]	1570	His, ν(C=C)	[42]
1113	$\tau(NH_2)$	[36]	1653	Amide I	[42]

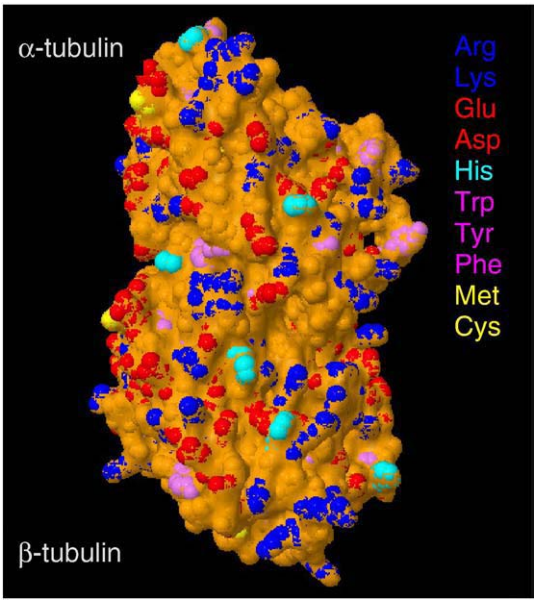

Fig. 3. Molecular surface of αβ-tubulin facing outside of MT. The crystal structure of the αβ-tubulin was obtained from www.pdb.org (PDB-code: 1tub) [47]. Amino acids with functional groups identified in SERS spectrum are colored with software Jmol-11.2.3. The rest of the protein surface is colored in orange brown.

speed used for concentrating Au nanoparticles was 14,000 rpm. The second control sample consisted of only MTs in solution. The sample was prepared by mixing 20 µl of 2.7 mg/ml MT in the pH 6.8 buffer described above, 20 µM taxol and 5 mM TX-100. This was then directly deposited on a piece of Si wafer and dried in air.

2.4. Raman spectroscopy measurements

Raman spectra were obtained using a Jobin-Yvon HR 640 triple monochromator equipped with a CCD. The 676.4 nm line of a Coherent I-300 Krypton ion laser (100 mW) was used for excitation.

2.5. Sample preparation for XPS

The sensitivity of the XPS measurement is such that we did not need multiple UV irradiation treatments to grow the Au nanoparticles. Thus, the Au decorated MT samples for XPS measurements were those obtained after the first UV irradiation. The Au MT pellet was concentrated and deposited on a 1 cm × 0.4 cm Ag coated Si wafer. Similarly, the control samples of Au nanoparticles were those obtained after the first UV irradiation. The washed and concentrated Au nanoparticles were deposited on a Ag coated Si wafer. The MT control sample was prepared by incubating 50 µl of 2.7 mg/ml MT solution on a piece of 1 cm × 0.4 cm Si wafer for 10 min. The Si wafer was then gently rinsed with distilled water several times and dried in air.

2.6. XPS measurements

The XPS measurements were performed in the analysis chamber of an Omicron XPS/UPS system. The base pressure of the chamber is better than 10^{-9} mbar. Al Kα (1486.6 eV) was used as the excitation source. The XPS spectra were deconvoluted with a combination of Gaussian and Lorentian fitting using XPSPEAK41 software.

3. Results and discussion

3.1. Au deposition on MTs

Au decorated MTs were fabricated using photochemical reactions in a solution containing MT, TX-100 and PIPES buffer. UV irradiation of the mixture produced Au nanoparticles and the solution turned from faint yellow to salmon red. A typical UV/vis spectrum taken from the solution 5 min after the UV irradiation showed a peak at 520 nm, indicating the formation of Au nanoparticles (Fig. 1A inset). TEM images of the sample 2 h after UV irradiation showed that 5–10 nm Au nanoparticles uniformly attached to the surface of MTs (Fig. 1A). The Au coverage can be further improved by a second photochemical reaction (Fig. 1B). The electron diffraction pattern obtained for this sample shows that these Au nanoparticles are polycrystalline (Fig. 1B inset). TX-100 micelle formation around the Au particle is thought to limit Au particle growth [32]. However, by using a higher concentration of $HAuCl_4$ (10 mM) and

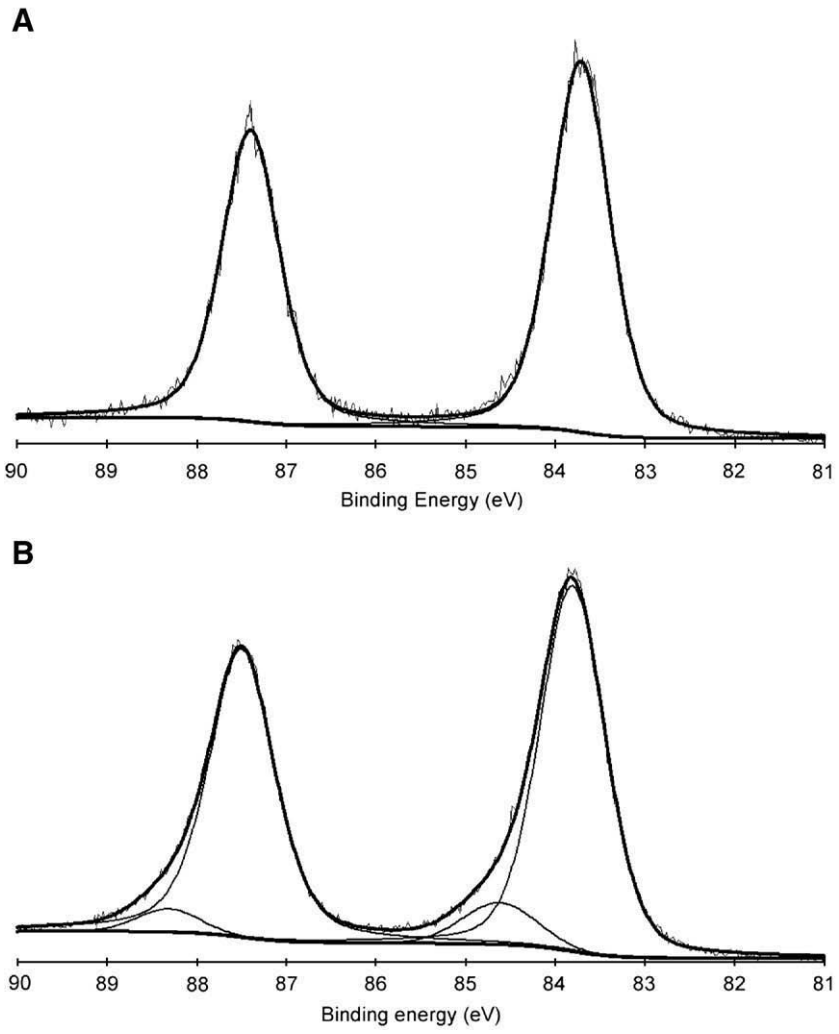

Fig. 4. Deconvolution of XPS spectra of the Au 4f lines. (A) Au nanoparticles formed by photochemical reduction. (B) Au decorated MT.

no TX-100, Au growth is no longer restricted and the Au nanoparticles can grow to 40 nm after a third UV irradiation (Fig. 1C). These samples are important for the SERS measurements because the aggregation of colloids tends to give a better SERS signal [33–35].

3.2. Surface enhanced Raman spectroscopy (SERS)

SERS is one of the most powerful techniques for characterizing the interaction between metal and protein functional groups. The excitation of surface plasmons on roughened metal surfaces such as Ag, Au and Cu selectively enhances (up to 10^9 times) the vibrational modes of only those molecules in close proximity to the roughened metal surface [34]. Thus, SERS offers very sensitive detection of the functional groups adsorbed on these metals. There have been several studies involving the use of SERS to determine the interaction between Au colloids and biomolecules [36–40]. In most of these investigations, however, the SERS studies emphasized the adsorption of single amino acids or short peptides which contain only a few potential binding sites.

In using SERS measurements to identify the functional groups on the MT surface that bind to the gold nanoparticles, it was necessary to have two separate control samples. The first control sample contained MT with TX-100 and PIPES buffer. The Raman spectrum for this sample exhibited no peaks except for those caused by the excitation laser (Fig. 2A, blue line) because the amount of MT, TX-100 and PIPES contained in this sample was too low to obtain sufficient Raman intensity. The second control sample contained Au nanoparticles formed photochemically in the presence of TX-100 and PIPES buffer. The SERS spectrum contained peaks at 750 cm^{-1}, 825 cm^{-1}, 1123 cm^{-1}, 1184 cm^{-1} and 1401 cm^{-1} (Fig. 2A, red line). The 750 cm^{-1}, 825 cm^{-1}, 1123 cm^{-1} and 1184 cm^{-1} vibrations are consistent with vibrational modes for TX-100 in solution [41]. No vibrations from the PIPES buffer were observed. Thus, these results indicate the presence of TX-100 on the Au nanoparticle surface, but not the PIPES buffer. That is, this work supports the scheme proposed by Zhu et al. [32] in which TX-100 coats the Au nanoparticle.

The SERS spectrum of the Au decorated MT sample had an additional twenty-four peaks (Fig. 2A, black line), which should all be due to the interactions between the functional groups on the MT and the Au surface. The region between 1500 cm^{-1} and 1590 cm^{-1} is magnified in Fig. 2B in order to show in greater detail that the vibrational modes are indeed enhanced in the Au decorated MTs as compared to the two control samples. All the enhanced peaks in Fig. 2A are listed in Table 1 and vibrational modes are assigned according to a previous Raman study of amino acids [42–44] and to SERS studies in which amino acids, short peptides, and biofunctional moieties were adsorbed on gold nanoparticles [36,37,39,40,42,45,46]. The different functional groups identified in these studies included imidazole, sulfur, carboxylate, aromatic ring and amine.

Histidine residues containing the imidazole group are probably the most prominent contributor to the Au binding. The crystal structure of αβ-tubulin dimers [47] (Fig. 3) shows that there are four histidines centrally located on the tubulin surface which are easily accessible

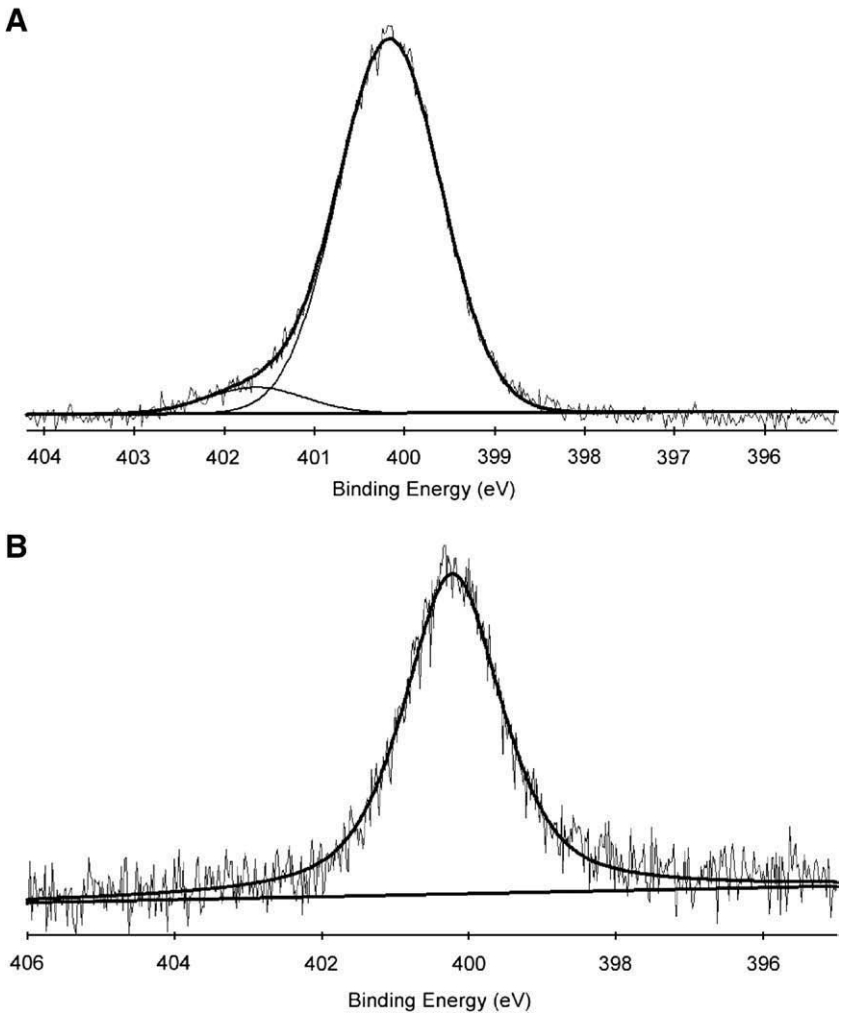

Fig. 5. Deconvolution of XPS spectra of the N 1s lines. (A) MTs. (B) Au decorated MT.

from the solution. The binding of gold to histidine residues is expected to occur primarily through the imidazole ring. Imidazole groups are well known to coordinate to a variety of metal ions in biological reactions. Histidine-rich peptides have been shown to reduce Au^{3+} and bind to gold nanoparticles [6,48]. At physiological pH, the δ imine in the imidazol ring is deprotonated, while the ε imine is usually protonated [49]. It is generally accepted that histidine coordinates through the basic δ imine and sometimes through the ε imine nitrogen center of the imidazole ring [49].

Sulfur is well known for forming stable covalent bonds with gold. However, the crystal structure of the αβ-tubulin dimers shows that only a small number of sulfur-containing cysteine and methionine residues are present on the outer surface of the MT. Moreover, because those moieties are not centrally located on the outer surface, they are not easily accessible to the gold solution. Thus, only a limited amount of gold–sulfur binding is expected.

The SERS spectrum also showed vibrational modes of amine, carboxylate and aromatic groups. These chemical moieties are usually not considered to be strong Au binding ligands. However, because of the vast number of these ligands on the MT surface, they are expected to contribute to the Au binding. The most abundant amino acid residues are negatively charged glutamate and aspartate containing a carboxylate group, but there are also a large number of positively charged amine-containing lysine and arginine. In addition, there is considerable evidence that aromatic ring-containing amino acids including tryptophan, tyrosine and phenylalanine interact with Au.

3.3. XPS analysis

We also used XPS to characterize the binding of Au to MT filaments. These measurements were particularly helpful in identifying the means by which Au interacts with primary amines.

The XPS spectrum of the Au 4f region is shown in Fig. 4. For the control sample of Au nanoparticles, the Au $4f_{7/2}$ and Au $4f_{5/2}$ levels give rise to peaks positioned at 83.7 eV and 87.4 eV respectively, consistent with the value of pure Au [50,51]. In contrast, the XPS spectrum for Au nanoparticles bound to MTs showed the presence of additional peaks of lower intensity that are positioned 0.8 eV higher in binding energy than the main peaks. Since we did not observe any Cl peak, we exclude the possibility that there was residual $HAuCl_4$ precursor on the surface. The fact that the second peaks occur at higher binding energy indicates that some Au atoms were oxidized upon binding to MTs.

The other XPS spectrum of interest is the N 1s region of the MT. Deconvolution of the XPS spectrum for the control MT sample gives rise to two peaks as shown in Fig. 5A. The position of the main peak at 400.2 eV is consistent with the N 1s core level binding energy. A second peak of much smaller magnitude and centered at 401.6 eV was

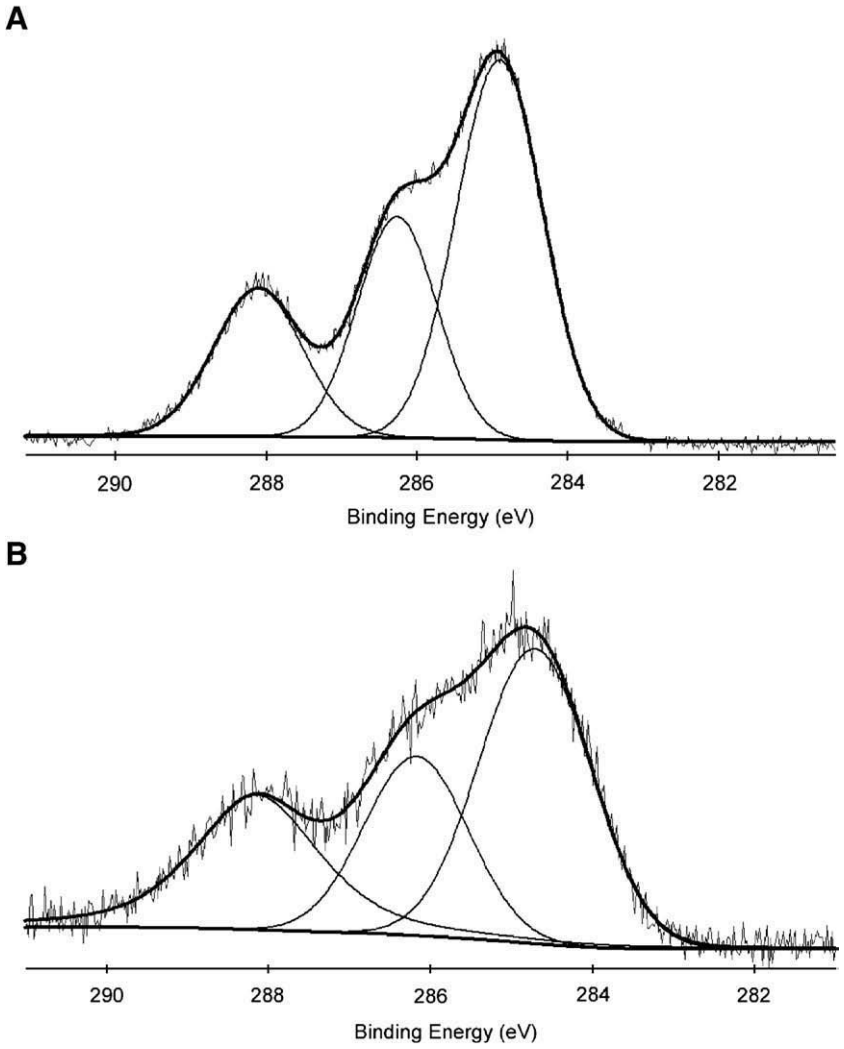

Fig. 6. XPS spectra of C 1s region for (A) MTs and (B) Au decorated MT.

assigned as protonated amine [51,52]. In the sample of Au bound MTs, the peak at the higher binding energy disappeared (Fig. 5B), leaving a single peak at 400.2 eV. The loss of the higher binding energy peak could be an indication that Au is adsorbed onto positively charged amine, donating electrons to nitrogen and decreasing the oxidation number on the nitrogen. Shifting the binding energy of N 1s to a lower level has also been observed for DNA chemisorbed onto Au surfaces via a thymine ring [53].

It is interesting to note that no peak was obtained from the S region around 162 eV. There are two possible sources of sulfur: from sulfur-containing residues on MT and the PIPES buffer. We did not expect to observe sulfur from the former because of the low content of these functional groups. Rather, the absence of the S peaks was a good indication that PIPES buffer was not present on the sample. PIPES buffer, which was used to provide a native environment for the MT, contains two SO_3^{2-} groups in each molecule. The absence of the S peak indicated that SO_3^{2-} is not strongly associated with Au and the MTs and can be easily removed by rinsing. This result was also consistent with the SERS spectrum for Au nanoparticles (Fig. 2) which does not exhibit any peaks associated with PIPES.

The C 1s line is another prominent feature in the XPS of MTs. In the control sample, the C 1s line can be resolved into three main components (Fig. 6A). The protein carbon backbone C–C and C–H are located at 284.9 eV [52,54], while the peak centered at 286.3 eV should be a combination of C–N and C–OH components [52,54]. The peak at 288.1 eV represents the binding energy of C in a combination of carboxylate (COO^-) [45,52] and amide (N–C=O) bonds [52,54]. Upon Au binding to the MT, these peaks appeared to be broadened (Fig. 6B), suggesting that chemical interaction with Au leads to shifts in the C binding energy. However, because of the presence of several possible interactions, no specific conclusions can be drawn.

4. Conclusions

The present study characterized the binding between the Au nanoparticles and microtubules using SERS and XPS. SERS revealed that the binding occurs through various functional groups on surface of the MTs. Among these functional groups, histidines are the most important residues for the binding because they are centrally located on the tubulin surface and they are well suited for Au coordination. There is also evidence that gold binding occurs through chemical moieties which are not considered to be strong Au binding ligands, but are nonetheless prominent on the MT surface. These functional groups including carboxylates, amines and aromatic rings, arise from various amino acid residues on the MT surface. XPS provides complementary information related to amine binding to the gold with the possible mechanism involving nitrogen atoms accepting electrons from the Au. The SERS studies also indicated the adsorption of TX-100 on the Au surface. This feature could lead to poor contact between Au particles and account for the lower electrical conductivity of the templated Au nanowires.

Acknowledgements

The authors acknowledge the financial and program support of the Microelectronics Advanced Research Corporation (MARCO) and its Focus Center on Functional Engineered Nano Achitectonics (FENA). We greatly appreciate the insightful comments of Professor Jeffrey I. Zink. We also thank Dr. Sergey Prikhodko for his help in obtaining the electron diffraction pattern.

References

[1] P.A. Smith, C.D. Nordquist, T.N. Jackson, T.S. Mayer, Appl. Phys. Lett. 77 (2000) 1399–1401.
[2] C.M. Niemeyer, Angew. Chem., Int. Ed. 40 (2001) 4128–4158.
[3] Q. Gu, C. Cheng, R. Gonela, S. Suryanarayanan, S. Anabathula, K. Dai, D.T. Haynie, Nanotechnology 17 (2006) R14–25.
[4] P. Deymier, Advanced Packaging, March 1 2004, pp. 15–16.
[5] S. Sotiropoulou, Y. Sierra-Sastre, S.S. Mark, C.A. Batt, Chem. Mater. 20 (2008) 821–834.
[6] R. Djalali, Y.-F. Chen, H. Matsui, J. Am. Chem. Soc. 124 (2002) 13660–13661.
[7] M. Reches, E. Gazit, Science 300 (2002) 625–627.
[8] A. Satti, D. Aherne, D. Fitzmaurice, Chem. Mater. (Comm.) 19 (2007) 1543–1545.
[9] G. Braun, K. Inagaki, R.R. Estabrook, D.K. Wood, E. Levy, A.N. Cleland, G.F. Strouse, N.O. Reich, Langmuir 21 (2005) 10699–10701.
[10] C. Mao, D.J. Solis, B.D. Reiss, S.T. Kottmann, R.Y. Sweeney, A. Hayhurst, G. Georgiou, B. Iverson, A.M. Belcher, Science 303 (2004) 213–217.
[11] C. Mao, C.E. Flynn, A. Hayhurst, R. Sweeney, J. Qi, G. Georgiou, B. Iverson, A.M. Belcher, Proc. Natl. Acad. Sci. 100 (2003) 6946–6951.
[12] S.W. Lee, C. Mao, C.E. Flynn, A.M. Belcher, Science 296 (2002) 892–895.
[13] Y. Huang, C.-Y. Chiang, S.K. Lee, Y. Gao, E.L. Hu, J.D. Yoreo, A.M. Belcher, Nano Lett. 5 (2005) 1429–1434.
[14] E. Dujardin, C. Peet, G. Stubbs, J.N. Culver, S. Mann, Nano Lett. 3 (2003) 413–417.
[15] W. Shenton, T. Douglas, M. Young, G. Stubbs, S. Mann, Adv. Mater. 11 (1999) 253–256.
[16] M.T. Kumara, B.C. Tripp, S. Muralidharan, Chem. Mater. 19 (2007) 2056–2064.
[17] T. Scheibel, R. Parthasarathy, G. Sawicki, X.-M. Lin, H. Jaeger, S.L. Lindquist, Proc. Natl. Acad. Sci. 100 (2003) 4527–4532.
[18] T.D. Pollard, W.C. Earnshaw, *Cell Biology*, Saunders, Philadelphia, 2002, pp. 579–593.
[19] S. Behrens, J. Wu, W. Habicht, E. Unger, Chem. Mater. 16 (2004) 3085–3090.
[20] S. Behrens, E. Unger, in: J.A. Schwarz, C.I. Contescu, K. Putyera (Eds.), *Dekker Encyclopedia of Nanoscience and Nanotechnology*, Marcel Dekker, Inc, New York, 2004, pp. 2563–2569.
[21] R. Bekeredjian, S. Behrens, J. Ruef, E. Dinjus, E. Unger, M. Baum, H.F. Kuecherer, Ultrasound Med. Biol. 28 (2002) 291–295.
[22] A.K. Boal, T.J. Headley, R.G. Tissot, B.C. Bunker, Mat. Res. Soc. Proc 823 (2004) W4.3.1–W4.3.6.
[23] S. Behrens, K. Rahn, W. Habicht, K.-J. Bohm, H. Rosner, E. Dinjus, E. Unger, Adv. Mater. 14 (2002) 1621–1625.
[24] R. Kirsch, M. Mertig, W. Pompe, R. Wahl, G. Sadowski, K.J. Bohm, E. Unger, Thin Solid Films 305 (1997) 248–253.
[25] M. Mertig, R. Kirsch, W. Pompe, Appl. Phys. A 66 (1998) S723–S727.
[26] J.C. Zhou, Y. Gao, A.A. Martinez-Molares, X. Jing, D. Yan, J. Lau, T. Hamasaki, C.S. Ozkan, M. Ozkan, E. Hu, B. Dunn, Small 4 (2008) 1507–1515.
[27] K. Mallick, X.L. Wang, T. Pal, J. Photochem. and Photobio. 140 (2001) 75–80.
[28] A. Pal, Talanta 46 (1998) 583–587.
[29] J.A. Cowan, *Inorganic Biochemistry: an Introduction*, VCH Publishers, Inc, New York, 1993, pp. 1–45.
[30] L.C. Ciacchi, M. Mertig, R. Seidel, W. Pompe, A.D. Vita, Nanotechnology 14 (2003) 840–848.
[31] R.C. Williams, J.C. Lee, in: L.W. Cunningham, D.W. Frederiksen (Eds.), *Methods in Enzymology*, vol. 85, Academic Press, New York, 1982, pp. 376–392.
[32] K. Zhu, L. Huang, J. Zhu, Z. Zhuang, Spectrochim. Acta, Part A 69 (2008) 566–571.
[33] I.W. Sztainbuch, J. Chem. Phys. 125 (2006) 124707–124712.
[34] W.E. Smith, C. Rodger, in: J.M. Chalmers, P.R. Griffiths (Eds.), *Handbook of Vibrational Spectroscopy*, vol. 1, John Wiley & Sons Ltd, Chichester; New York, 2002, pp. 775–784.
[35] J. Wang, T. Zhu, X. Zhang, Z. Liu, Acta Physioco-Chimica Sinica 15 (1999) 476–480.
[36] A.A. Ooka, R.L. Garrel, Biopolymers 57 (1999) 92–102.
[37] A.A. Ooka, K.A. Kuhar, N. Cho, R.L. Garrel, Biospectrosctroscopy 5 (1999) 9–17.
[38] A.H. Pakiari, Z. Jamshidi, J. Phys. Chem. A 111 (2007) 4391–4396.
[39] E. Podstawka, Y. Ozaki, L.M. Proniewicz, Appl. Spectrosc. 59 (2005) 1516–1526.
[40] H. Zhao, B. Yuan, X. Dou, J. Opt. A, Pure Appl. Opt. 6 (2004) 900–905.
[41] R.P. Cooney, C.G. Barraclough, T.W. Healy, J. Phys. Chem. 87 (1983) 1868–1873.
[42] T. Kitagawa, S. Hirota, in: J.M. Chalmers, P.R. Griffiths (Eds.), *Handbook of Vibrational Spectroscopy*, vol. 5, John Wiley & Sons Ltd, Chichester; New York, 2002, pp. 3426–3446.
[43] B.J.M. Rajkumar, V. Ramakrishnan, Spectrochim. Acta, Part A 58 (2002) 1923–1934.
[44] S. Hashimoto, H. Takeuchi, J. Am. Chem. Soc. 120 (1998) 11012–11013.
[45] S.W. Han, S.W. Joo, T.H. Ha, Y. Kim, K. Kim, J. Phys. Chem. B 104 (2000) 11987–11995.
[46] G.R. Souza, C.S. Levin, A. Hajitou, R. Pasqualini, W. Arap, J.H. Miller, Anal. Chem. 78 (2006) 6232–6237.
[47] E. Nogales, M. Whittataker, R.A. Milligan, K.H. Downing, Cell 96 (1999) 79–88.
[48] J.M. Slocik, J.T. Moore, D.W. Wright, Nano Lett. 2 (2002) 169–173.
[49] W. Kaim, B. Schwederski, *Bioinorganic Chemistry: Inorganic Elements in the Chemistry of Life*, John Wiley & Sons Ltd, Chichester; New York, 1994, pp. 6–38.
[50] S. Dieluweit, D. Pum, U.B. Sleytr, W. Kautek, Mater. Sci. Eng 25 (2005) 727–732.
[51] G. Dodero, L.D. Michieli, O. Cavalleri, R. Rolandi, L. Oliveri, A. Dacca, R. Parodi, Colloids Surf., A: Physicochem. Eng. Asp. 175 (2000) 121–128.
[52] R.J. Tseng, C. Tsai, L. Ma, J. Ouyang, C.S. Ozkan, Y. Yang, Nat. Nanotechnol. 1 (2006) 72–77.
[53] D.Y. Petrovykh, H. Kimura-Suda, L.J. Whitman, M.J. Tarlov, J. Am. Chem. Soc. 125 (2003) 5219–5226.
[54] C.J. May, H.E. Canavan, D.G. Castner, Anal. Chem. 76 (2004) 1114–1122.